PHYSICAL REVIEW C **84**, 062802(R) (2011)

Masses of neutron stars and nuclei

N. Chamel,[1] A. F. Fantina,[1] J. M. Pearson,[2] and S. Goriely[1]
[1]*Institut d'Astronomie et d'Astrophysique, CP-226, Université Libre de Bruxelles, B-1050 Brussels, Belgium*
[2]*Département de Physique, Université de Montréal, Montréal, Québec, H3C 3J7 Canada*
(Received 13 October 2011; revised manuscript received 22 November 2011; published 15 December 2011)

We calculate the maximum mass of neutron stars for three different equations of state (EOSs) based on generalized Skyrme functionals that are simultaneously fitted to essentially all the 2003 nuclear mass data (the rms deviation is 0.58 MeV in all three cases) and to one or other of three different equations of state of pure neutron matter, each determined by a different many-body calculation using realistic two- and three-body interactions but leading to significantly different degrees of stiffness at the high densities prevailing in neutron-star interiors. The observation of a neutron star with mass $1.97 \pm 0.04\ \mathcal{M}_\odot$ eliminates the softest of our models (BSk19), but does not discriminate between BSk20 and BSk21. However, nuclear-mass measurements that have been made since our models were constructed strongly favor BSk21, our stiffest functional.

DOI: 10.1103/PhysRevC.84.062802 PACS number(s): 21.10.Dr, 21.65.Cd, 21.65.Mn, 26.60.Dd

The nuclear energy-density functional theory aims at describing various nuclear systems containing a large number of nucleons. It has been very successfully applied to the study of the structure and the dynamics of medium-mass and heavy nuclei [1]. This approach is also particularly well suited to the determination of the properties of dense nuclear matter in extreme astrophysical environments such as supernova cores and neutron-star interiors [2]. In this framework we recently constructed a family of three functionals, BSk19, BSk20, and BSk21 [3], each one intended to provide a unified approach to the description not only of the different regions of neutron stars (including the possibility of superfluidity [4]) but also of supernova cores. These functionals have all been derived from Skyrme forces of the form

$$\begin{aligned} v_{ij} &= t_0(1+x_0P_\sigma)\delta(\boldsymbol{r}_{ij}) \\ &+ \frac{1}{2}t_1(1+x_1P_\sigma)\frac{1}{\hbar^2}\left[p_{ij}^2\,\delta(\boldsymbol{r}_{ij}) + \delta(\boldsymbol{r}_{ij})\,p_{ij}^2\right] \\ &+ t_2(1+x_2P_\sigma)\frac{1}{\hbar^2}\boldsymbol{p}_{ij}\delta(\boldsymbol{r}_{ij})\,\boldsymbol{p}_{ij} \\ &+ \frac{1}{6}t_3(1+x_3P_\sigma)\,n(\boldsymbol{r})^\alpha\,\delta(\boldsymbol{r}_{ij}) \\ &+ \frac{1}{2}\,t_4(1+x_4P_\sigma)\frac{1}{\hbar^2}\left[p_{ij}^2\,n(\boldsymbol{r})^\beta\,\delta(\boldsymbol{r}_{ij}) + \delta(\boldsymbol{r}_{ij})\,n(\boldsymbol{r})^\beta\,p_{ij}^2\right] \\ &+ t_5(1+x_5P_\sigma)\frac{1}{\hbar^2}\boldsymbol{p}_{ij}n(\boldsymbol{r})^\gamma\,\delta(\boldsymbol{r}_{ij})\,\boldsymbol{p}_{ij} \\ &+ \frac{\mathrm{i}}{\hbar^2}W_0(\boldsymbol{\sigma_i}+\boldsymbol{\sigma_j})\cdot\boldsymbol{p}_{ij}\times\delta(\boldsymbol{r}_{ij})\,\boldsymbol{p}_{ij}, \end{aligned} \tag{1}$$

where $\boldsymbol{r}_{ij} = \boldsymbol{r}_i - \boldsymbol{r}_j, \boldsymbol{r} = (\boldsymbol{r}_i + \boldsymbol{r}_j)/2$, $\boldsymbol{p}_{ij} = -\mathrm{i}\hbar(\boldsymbol{\nabla}_i - \boldsymbol{\nabla}_j)/2$ (this is the relative momentum), P_σ is the two-body spin-exchange operator, and $n(\boldsymbol{r}) = n_n(\boldsymbol{r}) + n_p(\boldsymbol{r})$ is the total local density, $n_n(\boldsymbol{r})$ and $n_p(\boldsymbol{r})$ being the neutron and proton densities, respectively. These forces are generalizations of the conventional Skyrme form in that they contain terms in t_4 and t_5, which are density-dependent generalizations of the usual t_1 and t_2 terms, respectively [5].

The parameters of this form of force were determined primarily by fitting measured nuclear masses, which were calculated with the Hartree-Fock-Bogoliubov (HFB) method. For this it was necessary to supplement the Skyrme forces with a microscopic contact pairing force, phenomenological Wigner terms, and correction terms for the spurious collective energy. However, in fitting the mass data we simultaneously constrained the Skyrme force to fit the zero-temperature equation of state (EOS), i.e., the energy per nucleon e as a function of the density n, of homogeneous pure neutron matter (NeuM), as determined by many-body calculations with realistic two- and three-nucleon forces. Actually, several such calculations of the EOS of NeuM have been made, and while they all agree very closely at nuclear and subnuclear densities, at the much higher densities that can be encountered toward the center of neutron stars they differ greatly in the stiffness that they predict. It is in this way that we arrived at the three different effective forces of this paper: BSk19 was fitted to the softest EOS of NeuM known to us, that of FP [6] and the one labeled "UV14 plus TNI" in Ref. [7] and which we refer to as WFF, BSk21 to the stiffest, the one labeled "V18" in Ref. [8] and which we refer to as LS2, while BSk20 was fitted to an EOS of intermediate stiffness, the one labeled "A18 $+\,\delta\,v+$ UIX*" in Ref. [9] and which we refer to as APR (see Fig. 1). Furthermore, the strength of the pairing force at each point in the nucleus in question was determined so as to exactly reproduce realistic $^1S_0$ pairing gaps of homogeneous nuclear matter of the appropriate density and charge asymmetry [10]. Finally, we imposed on these forces a number of supplementary realistic constraints, the most notable of which is the suppression of an unphysical transition to a spin-polarized configuration both at zero and finite temperatures, at densities found in neutron stars and supernova cores [3,5,11].

The introduction of the unconventional Skyrme terms allowed us to satisfy all these constraints and at the same time fit the 2149 measured masses of nuclei with N and $Z \geqslant 8$ given in the 2003 Atomic Mass Evaluation (AME) [12] with an rms deviation as low as 0.58 MeV for all three models, i.e., for all three options for the high-density behavior of NeuM. Fig. 1 also shows the EOS in NeuM of Skyrme force SLy4 [13]. This force, like our own, was intended for use in neutron stars.

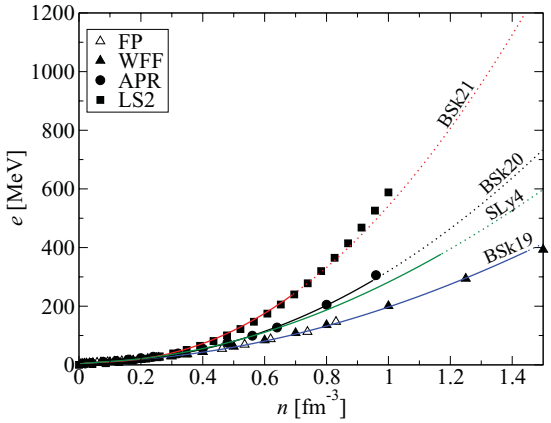

FIG. 1. (Color online) Zero-temperature EOSs for neutron matter (NeuM) with functionals of this Rapid Communication. Also shown are the realistic EOSs FP [6], WFF [7], APR [9], and LS2 [8]. Dotted curves denote supraluminal EOS.

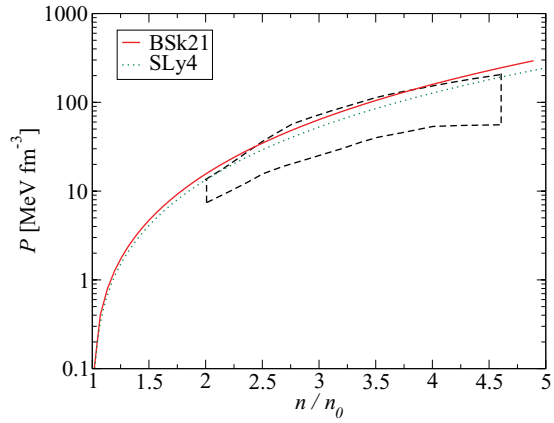

FIG. 3. (Color online) Calculated pressures in symmetric nuclear matter (SNM) for functionals of this paper (BSk19 and BSk20 yield almost undistinguishable results from BSk21 on this figure); the box summarizes the range of the measurements reported in Ref. [15].

We see that its EOS in NeuM lies between those of BSk19 and BSk20, i.e., between the realistic EOSs of FP-WFF and APR. It was also fitted to a few nuclear masses, but the overall quality of the fit is rather poor, an rms deviation of 5.1 MeV for all the measured even-even nuclei being quoted [14].

Neutron-star structure. With each of our functionals we have calculated the zero-temperature EOS in each of the three regions of neutron stars. In Ref. [3] we calculated the EOS of neutron-star matter (N*M), the medium constituting the homogeneous core (assumed here to consist of just neutrons, protons, electrons and muons), which dominates the global properties of neutron stars. Referring to Fig. 2, we see that qualitatively, the EOS of N*M resembles that of NeuM for the same force, with BSk19 still having the softest EOS and BSk21 the stiffest. Figure 2 also shows the EOS of functional SLy4 in N*M.

Aside from the obvious influence of the leptons, the main reason for the differences between the EOS of NeuM and that of N*M lies in the presence of protons, which interact both with each other and with neutrons. The precision mass fit

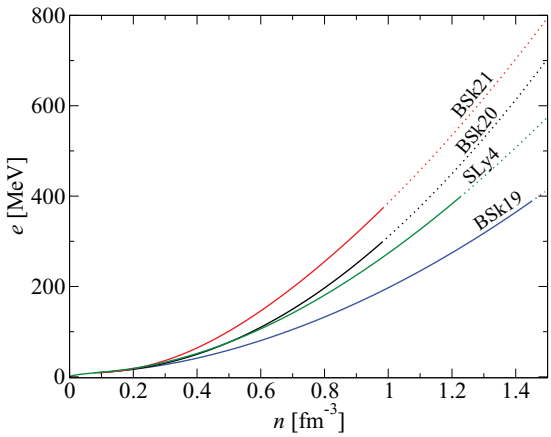

FIG. 2. (Color online) Zero-temperature EOSs for neutron-star matter (N*M) with functionals of this paper. Dotted curves denote supraluminal EOS.

assures that these interactions are well represented, at least up to densities not much greater than n_0, the equilibrium density of symmetric nuclear matter (SNM). As for higher densities, the extent to which the EOS of N*M is not determined by that of NeuM depends on the EOS of SNM, and as can be seen in Fig. 3, our models are consistent with measurements of the high-density pressure of SNM deduced from heavy-ion collisions [15], even though our functionals were not directly fitted to the EOS of SNM. Thus, all in all, we believe that the procedure for determining our forces has an optimal mix of theory and experiment, at least as far as the EOS of N*M is concerned.

Our functionals are equally well adapted to the calculation of the EOS of the neutron-star crust. For the outer part of the crust, consisting of just electrons and bound nuclei, we used the HFB-19, HFB-20, and HFB-21 mass models [16], whenever experimental masses are not available. These are based entirely on the BSk19, BSk20, and BSk21 parameters, respectively, and were constructed to run from one drip line to the other [3]. Given not only the precision fit that these models give to the measured masses but also the constraints to NeuM imposed on the underlying forces, no other published mass model will make more reliable predictions for the experimentally inaccessible neutron-rich nuclei that dominate the outer crust. (For the same reason these mass models are well adapted to the study of the r-process of nucleosynthesis [17,18].) For the inner crust, which consists of neutron-proton clusters embedded in a neutron vapor and electron gas, we have likewise calculated the EOS with each of the BSk19, BSk20, and BSk21 functionals, using the ETFSI (extended Thomas-Fermi plus Strutinsky integral) method [19]. Our confidence in the use of our functionals in this region derives not only from the NeuM constraints to which they have been subjected but also from the precision fit to masses, which means that the presence of inhomogeneities and of protons is well represented.

For each of these three Skyrme functionals we thus have at our disposal the zero-temperature EOS for all parts of neutron stars, and hence can solve the Tolman-Oppenheimer-Volkoff

TABLE I. For each functional are shown (i) limiting baryonic density for causality, (ii) maximum neutron-star mass (the quantities in parentheses refer to the corresponding realistic forces), (iii) corresponding radius and (iv) corresponding central baryonic density. (Neutron-star results for SLy4 taken from Ref. [23].)

Force	$n_{\rm caus}$ (fm^{-3})	$\mathcal{M}_{\rm max}/\mathcal{M}_\odot$	R (km)	$n_{\rm cen}$ (fm^{-3})
BSk19	1.45	1.86 (1.84 [7])	9.13	1.45
BSk20	0.98	2.15 (2.20 [9])	10.6	0.98
BSk21	0.99	2.28 (2.3 [8])	11.0	0.98
SLy4	1.23	2.05	9.99	1.21

(TOV) equations describing the global structure of spherical nonrotating neutron stars [20,21]. Solving these equations for different values of the baryonic central density, $n_{\rm cen}$, gives us the total gravitational mass $\mathcal{M}$ as a function of the circumferential radius R. Numerical calculations have been carried out using the LORENE library [22]. The maximum possible value of $\mathcal{M}$, $\mathcal{M}_{\rm max}$, along with the corresponding radius R and central density $n_{\rm cen}$, are given in the last three columns of Table I for each of our three functionals. The second column of this table shows $n_{\rm caus}$, the maximum value of the baryonic density in N*M for which causality holds, i.e., for which the velocity of sound is lower than the velocity of light, c (see Sec. V B of Ref. [3] for details). It will be seen that for functionals BSk19 and BSk20 the central density $n_{\rm cen}$ for maximum mass is at the limit imposed by causality; in fact if we had waived this constraint we would have found slightly higher (and unphysical) values of $\mathcal{M}_{\rm max}$ and $n_{\rm cen}$ (the maximum mass would have been essentially the same for BSk19, whereas it would have increased to $\mathcal{M}_{\rm max} = 2.17\mathcal{M}_\odot$ for BSk20). On the other hand, in the case of functional BSk21, which has the stiffest EOS, the requirement of causality is satisfied for all possible masses. Table I also shows (in parentheses), for each of BSk19, BSk20, and BSk21, the value of $\mathcal{M}_{\rm max}$ that has already been published for the corresponding realistic calculation, i.e., WFF, APR, and LS2, respectively. The close agreement between corresponding values of $\mathcal{M}_{\rm max}$ is a measure of how well we have reproduced the realistic forces with our Skyrme functionals.

Comparing the values of $\mathcal{M}_{\rm max}$ shown in Table I with the recently measured value of $1.97 \pm 0.04\ \mathcal{M}_\odot$ for the mass of pulsar PSR J1614−2230 [24] shows that the EOS of BSk19 for N*M and NeuM is definitely too soft. Even taking account of the fact that this pulsar rotates with a frequency of 317 Hertz, we have found using the LORENE library [22] (considering stationary configurations for rigidly rotating neutron stars, see, e.g., Ref. [25]) that $\mathcal{M}_{\rm max}$ is raised only by $0.005\ \mathcal{M}_\odot$, which is insufficient to change this conclusion. On the other hand, functionals BSk20 and BSk21, along with SLy4, all provide EOSs that are sufficiently stiff to support PSR J1614−2230.

Referring to Fig. 4, we see that BSk21 is the only one of our functionals for which the proton fraction can exceed the critical threshold for a direct Urca process to occur, and then only for baryon density $n > 0.45$ fm^{-3}, i.e., only in neutron stars whose gravitational mass $\mathcal{M} > 1.59\mathcal{M}_\odot$. As a consequence, our three functionals are compatible with the constraint of Ref. [26] that no direct Urca process should occur in neutron stars with masses in the range 1–1.5 $\mathcal{M}_\odot$. However, we now see that recently accumulated nuclear-mass data strongly favor BSk21.

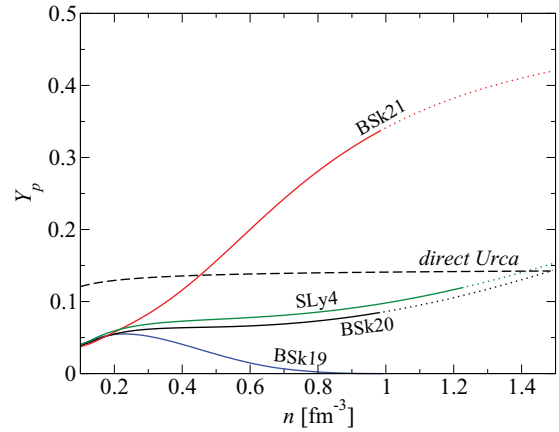

FIG. 4. (Color online) Proton fraction Y_p in neutron-star matter for functionals of this Rapid Communication. The dashed line indicates the threshold value of Y_p for the direct Urca process to be allowed. Dotted curves denote supraluminal EOS.

Nuclear masses. Since we fitted our forces to the data of the 2003 AME many new mass data have been accumulated. In particular, a new unpublished AME became available in 2011 [27]. This contains 154 new measurements in the interval N and $Z \geqslant 8$, while nine masses that were previously listed as "measured" have now been demoted to an "estimated" status;

TABLE II. Rms and mean deviations between mass models and different data sets (see text).

Data set	Number of nuclei	Mass model	rms (MeV)	$\bar{\epsilon}$ (MeV)
2003 AME	2149	HFB-19	0.583	−0.038
"	"	HFB-20	0.582	0.021
"	"	HFB-21	0.577	−0.054
2003 AME n-rich	185	HFB-19	0.803	0.243
"	"	HFB-20	0.790	0.217
"	"	HFB-21	0.762	−0.086
2011 AME	2294	HFB-19	0.595	−0.010
"	"	HFB-20	0.593	0.051
"	"	HFB-21	0.574	−0.031
2011 AME n-rich	224	HFB-19	0.799	0.261
"	"	HFB-20	0.788	0.255
"	"	HFB-21	0.730	−0.060
2011 new	154	HFB-19	0.824	0.310
"	"	HFB-20	0.803	0.375
"	"	HFB-21	0.681	0.185
2011 new n-rich	73	HFB-19	0.948	0.391
"	"	HFB-20	0.893	0.408
"	"	HFB-21	0.735	0.063
2007 Matos	17	HFB-19	0.912	0.757
"	"	HFB-20	0.878	0.713
"	"	HFB-21	0.536	0.216

in accordance with our previous practice we do not consider such nuclei.

The first three lines of Table II show the rms and mean deviations of our HFB-19, HFB-20, and HFB-21 mass models with respect to all measured masses in the interval N and $Z \geqslant 8$ in the 2003 AME, while the next three lines show the corresponding results for the subset consisting of nuclei with a neutron separation energy of less than 5.0 MeV. A slight favoring of HFB-21 over the other two models is already apparent in this neutron-rich domain, the region of interest in neutron-star applications. This trend is strengthened somewhat in the next six lines, where we show the corresponding results for the 2011 AME. Accordingly, in the next three lines (13 to 15) we look at the deviations with respect to just the 154 new data points: the discrimination in favor of HFB-21 is now quite marked, although both neutron-rich and proton-rich nuclei are included in this set. Of these 154 new nuclei 73 lie on the neutron-rich side of the stability line, and we show the corresponding deviations in lines 16 to 18 of Table II. There is now an even stronger selection of HFB-21.

Not included in either AME are the 41 unpublished mass measurements of highly neutron-rich nuclei by Matos [28]. The 2011 AME lists 24 of these nuclei, and although the Matos data were not used the agreement is very good. We consider the subset of the remaining 17 Matos data in the last three lines of Table II, where we see further confirmation of a strong preference for HFB-21.

Conclusions. Our three nuclear mass models HFB-19, HFB-20, and HFB-21, which are based on the functionals BSk19, BSk20, and BSk21, respectively, give equally good fits to the nuclear mass data appearing in the 2003 AME [12]. However, since 2003, and since our mass models were fitted, mass measurements have begun to be made sufficiently far from the stability line to discriminate between our models. Specifically, model BSk21 is strongly favored by the new data.

To complement this conclusion we have solved the general-relativistic equations of rotating and non-rotating stars for our three functionals and find that BSk19 is too soft at high densities to support neutron stars as heavy as the heaviest yet observed, while BSk20 and BSk21 will. This corroboration between measurements of nuclear masses and measurements of neutron-star masses is gratifying, but it should not be concluded that nuclear-mass measurements are now tying down the high-density EOS of N*M, since with a more elaborate Skyrme parametrization (e.g., by taking several forms of each of the t_3, t_4, and t_5 terms) it might be possible to have an equally good fit to all the mass data while making different extrapolations to high-density N*M. Nevertheless, at the very least we recognize that in BSk21 we have a functional that performs well over a wide range of densities, giving a precision fit to nuclear masses, and being compatible with what is now known about neutron-star masses.

Acknowledgments. We would like to thank M. Matos for sending us his thesis results, and G. Audi, P. Haensel, and D. Lunney for valuable communications. The financial support of the FNRS (Belgium), the NSERC (Canada), and CompStar (a Research Networking Programme of the European Science Foundation) is gratefully acknowledged.

[1] M. Bender, P.-H. Heenen, and P.-G. Reinhard, Rev. Mod. Phys. **75**, 121 (2003).
[2] J. R. Stone and P. G. Reinhard, Prog. Part. Nucl. Phys. **58**, 587 (2007).
[3] S. Goriely, N. Chamel, and J. M. Pearson, Phys. Rev. C **82**, 035804 (2010).
[4] N. Chamel, S. Goriely, J. M. Pearson, and M. Onsi, Phys. Rev. C **81**, 045804 (2010).
[5] N. Chamel, S. Goriely, and J. M. Pearson, Phys. Rev. C **80**, 065804 (2009).
[6] B. Friedman and V. R. Pandharipande, Nucl. Phys. A **361**, 502 (1981)
[7] R. B. Wiringa, V. Fiks, and A. Fabrocini, Phys. Rev. C **38**, 1010 (1988).
[8] Z. H. Li and H.-J. Schulze, Phys. Rev. C **78**, 028801 (2008).
[9] A. Akmal, V. R. Pandharipande, and D. G. Ravenhall, Phys. Rev. C **58**, 1804 (1998).
[10] N. Chamel, Phys. Rev. C **82**, 014313 (2010).
[11] N. Chamel and S. Goriely, Phys. Rev. C **82**, 045804 (2010).
[12] G. Audi, A. H. Wapstra, and C. Thibault, Nucl. Phys. A **729**, 337 (2003).
[13] E. Chabanat, P. Bonche, P. Haensel, J. Meyer, and R. Schaeffer, Nucl. Phys. A **635**, 231 (1998); **643**, 441 (1998).
[14] J. Dobaczewski, M. V. Stoitsov, and W. Nazarewicz, AIP Conf. Proc. **726**, edited by R. Bijker, R. F. Casten, and A. Frank (American Institute of Physics, New York, 2004), p. 51.
[15] P. Danielewicz, R. Lacey, and W. G. Lynch, Science **298**, 1592 (2002).
[16] J. M. Pearson, S. Goriely, and N. Chamel, Phys. Rev. C **83**, 065810 (2011).
[17] S. Goriely, N. Chamel, H.-T. Janka, and J. M. Pearson, Astron. Astrophys. **531**, A78 (2011).
[18] S. Goriely, A. Bauswein, and H.-T. Janka, Astrophys. J. Lett. **738**, L32 (2011).
[19] J. M. Pearson, N. Chamel, S. Goriely, and C. Ducoin (submitted to Phys. Rev. C, 2011).
[20] R. C. Tolman, Phys. Rev. **55**, 364 (1939).
[21] J. R. Oppenheimer and G. M. Volkoff, Phys. Rev. **55**, 374 (1939).
[22] [http://www.lorene.obspm.fr.]
[23] F. Douchin and P. Haensel, Astron. Astrophys. **380**, 151 (2001).
[24] P. B. Demorest, T. Pennucci, S. M. Ransom, M. S. E. Roberts, and J. W. T. Hessels, Nature **467**, 1081 (2010).
[25] E. Gourgoulhon, lectures notes, arXiv:1003.5015.
[26] T. Klähn *et al.*, Phys. Rev. C **74**, 035802 (2006).
[27] G. Audi and M. Wang (private communication, 2011).
[28] M. Matos, Giessen doctoral thesis (unpublished, 2004).